Removal of Congo red and Brilliant green dye from aqueous solution using flower shaped ZnO nanoparticles

Navish Kataria[1] and V.K. Garg[1, 2,*]

[1]Department of Environmental Science and Engineering, Guru Jambheshwar University of Science and Technology, Hisar-125001, India
[2]Centre for Environmental Sciences and Technology, Central University of Punjab, Bathinda-151001, India

*Corresponding author: email: vinodkgarg@yahoo.com
Tel: +91-9812058109

Graphical abstract:

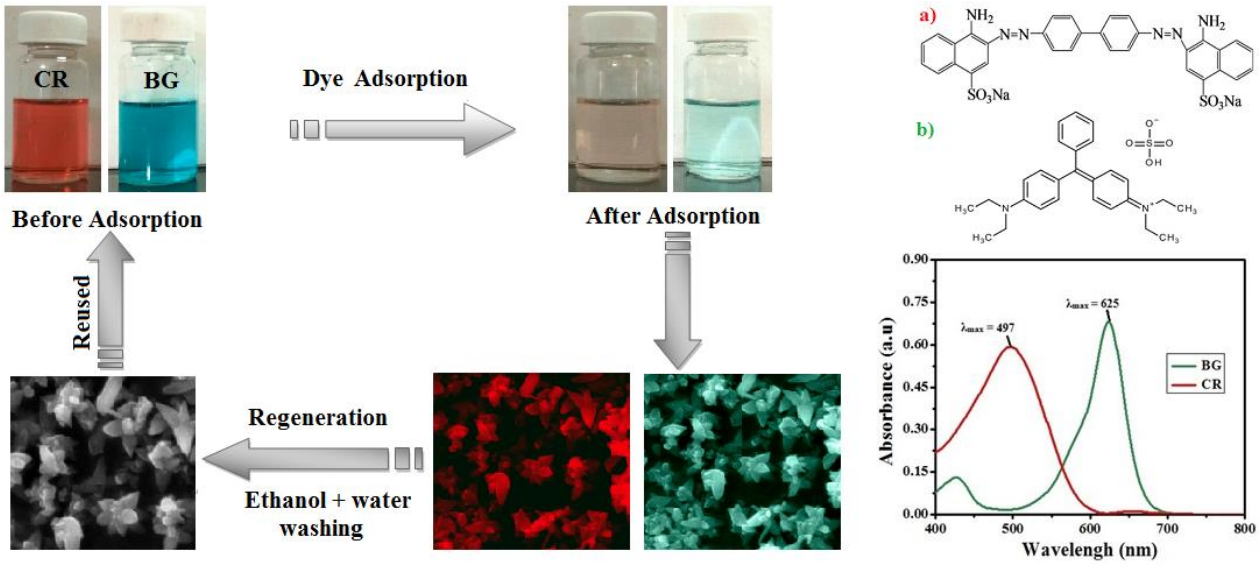

Highlights

- Zinc oxide nanoparticles were synthesized by low temperature hydrothermal method.
- Cationic and anionic dyes' removal has been investigated in batch mode .
- The maximum adsorption capacity for congo red and brilliant green dye onto ZnO nanoparticles was 71.4 mg/g and 238 mg/g respectively.
- ZnO nanoparticles may be reused for dye removal from aqueous solution.

Abstract

This work reports preparation and characterization of ZnO nanoparticlesnanoparticles prepared by low temperature hydrothermal methods and their application for anionic dye (Congo red) and cationic dye (Brilliant green) removal from aqueous smedium. The adsorption capacity of ZnO nanoparticles for Congo red dye and Brilliant green dye was up to 71.4 and 238 mg/g, respectively under selected process conditions. Dye adsorption behaviour has been explained applying different isotherms. Freundlich isotherm model best fitted to the dye removal data. Adsorption kinetics of both dyes is well explained by pseudo-second order model. Physical adsorption has been investigated using thermodynamic parameters viz., Gibb's free energy (ΔG^o), enthalpy (ΔH^o) and entropy (ΔS^o). The reusability of ZnO nanoparticles was examined upto three cycles.

Keywords: Flower shaped ZnO nanoparticles, Congo red, Brilliant green, Adsorption Isotherms, adsorption capacity, Kinetics.

Introduction

In recent year, aquatic environment is continually contaminated by anthropogenic pollutants including heavy metals, dyes, surfactants, pesticides etc. Organic dyes are commonly found in wastewater that is generated by industries such as textile, paper and pulp, printing, leather, pharmaceutical etc. [1]. Brilliant green (BG) dye is a cationic dye and may cause several health problems including skin and eye irritation, vomiting, diarrhoea, shortness of breath, coughing, nausea etc. [2,3]. Congo red (CR) dye is an anionic dye with complex aromatic structure which makes it stable against oxidizing agents and non-biodegradable. Therefore, it can exist in the environment for longer period [4]. Hence, treatment of industrial wastewater laden with such dyes before discharge is essential concern for researcher and industries due to stringent disposal regulation.

Several treatment technologies such as membrane separation, adsorption, photocatalytic, flocculation–coagulation, advance oxidation process, ozonation etc. are employed for wastewater treatment [5, 6]. Among these, adsorption is conventional and most preferable technology for the treatment of dye laden wastewater. In adsorption process,

highly efficient and low cost adsorbents make it economically, environmentally and technically sustainable approach for dye removal [7]. In recent years, attempts have been made to use as micro/nanostructure especially metal oxides nanoparticles for the treatment of wastewater. These metal oxides contain unique properties such as large surface area, high efficiency, chemically stability and surface functional groups. Therefore, these metal oxides could be good adsorbents and photo-catalysts for wastewater treatment [8]. ZnO is one among the promising material due to its environmental friendly nature and surface functional groups [9, 10]. In literature, several studies have been reported on photo-degradation of dye by metal oxides specially ZnO nanoparticles [11, 12]. But very few studies are available on ZnO nanoparticles as adsorbent for dye removal. ZnO micro/nanostructure synthesis using hydrothermal method is economically cheaper, easy to modify particle size and shape and higher yield of particles [7].

In the present work, ZnO nanoparticles were prepared by hydrothermal method. Its performance for CR and BG dye adsorption was assessed by batch mode experiments under different experimental conditions. The adsorption capacity and mechanism involve in the adsorption process were evaluated using isotherms models and kinetics. Further, reusability of ZnO nanoparticles for dyes removal was examined for three cycles.

2. Experiments

2.1. Materials & Reagents

Zinc nitrate hexahydrate [Zn $(NO_3)_3.6H_2O$] and Hexamethylenetetramine (HMTA) $[(CH_2)_6N_4]$ was procured from Himedia laboratory Pvt. Ltd., India. Sodium hydroxide (NaOH) pellets (AR grade); Congo red dye and Brilliant green dyes were procured from SD fine-chem Ltd, Mumbai. All chemicals used in the present study were AR grade. The physico-chemical characteristics of the CR and BG dyes are given in Table 1.

2.2. Synthesis and Characterization of ZnO nanoparticles (ZnO nanoparticles)

ZnO nanoparticles were synthesized by hydrothermal method as reported earlier by Kataria et al., [10]. Scheme of hydrothermal synthesised ZnO nanoparticles shown in Fig. 1 and reaction mechanism involved in ZnO nanoparticles synthesis is given below.

$$Zn(NO_3)_2.6H_2O \longrightarrow Zn^{2+} + 2NO_3^-$$

$$C_6H_{12}N_4 + 6H_2O \longrightarrow 4NH_3 + 6HCHO$$

$$NH_3 + H_2O \longleftrightarrow NH_4^+ + OH^-$$

$$Zn^{2+} + 2OH^- \longleftrightarrow Zn(OH)_2$$

$$Zn(OH)_2 \xrightarrow{\Delta} ZnO + H_2O$$

The molecular structure of synthesised ZnO nanoparticles was recorded by XRD (PANalytical X'Pert Pro Multipurpose Diffractometer), using Cu-K_α X-ray radiation (λ=1.5418 Å) at 40 kV and a current of 40 mA. Dynamic light scattering (DLS) technique was used to determine the size distribution of synthesized ZnO nanoparticles by Zetasizer. To know the presence of functional group FTIR spectrum were recorded. The surface morphology and elemental characteristics of ZnO nanoparticles were determined by Scanning electron microscope (SEM) and Energy-dispersive X-ray spectroscopy (EDX) techniques, respectively. The detailed of various instruments used for characterization of ZnO nanoparticles is reported earlier [10]. The specific surface area of ZnO nanoparticles was determined using the Brunauer–Emmett–Teller (BET) method using BET analyzer (Quantachrome Nova 2000e, USA). The pore size distribution was calculated by BJH theory based on nitrogen adsorption-desorption isotherm at 77.4 K.

2.3. Point of zero charge (pHpzc):

The point of zero charge (pHpzc) of ZnO nanoparticles was determined by salt addition technique. In this technique, 0.1g of the ZnO nanoparticles was added into 40 mL solution of $NaNO_3$ and initial pH (pHi) was maintained 3 to 10 using acid (0.1M HNO_3) and base (0.1M NaOH) solutions. The flasks were put in shaker for 48h at 27±1°C. After 48h shaking, the final pH (pHf) of the solution was determined using pH meter. The pHpzc of adsorbent was calculated by plots of ΔpH (pHf – pHi) versus pHi.

2.4. Adsorption experiments

This study was conducted in batch mode 0.04g adsorbent was added to 50ml of 50mg/L CR and BG dye solution. All adsorption experiments were conducted in orbital shaker under dark condition (Scigenics Biotech ORBITEK, India) in an Erlenmeyer flask at 27±1˚C with shaking speed 180 rpm. The pH of dye solution was adjusted by using HCl (0.1M) and NaOH (0.1M) solution using Cyber scan pH tutor (Eutech Instruments**,** Singapore). Dye concentration was quantified by UV-VIS spectrophotometer (UV-VIS 3000^+ LABINDIA, India). ZnO nanoparticles were separated from dye solution using centrifugation at 5000 rpm for 10 minutes. The absorbance of supernatant was recorded to find out residual

dye concentration at λ_{max} 497nm for CR and λ_{max} 625nm for BG dyes. Dye removal (%) and adsorption capacity was calculated by the following expression:

$$Dye\ removal\ (\%) = \frac{(C_o - C_e)}{C_o} \times 100 \quad (1)$$

$$Adsorption\ capacity\ (q_e) = \frac{(C_o - C_e)\,V}{m} \quad (2)$$

Where C_o (mg/L) is the initial concentration, C_e (mg/L) is the dye concentration at equilibrium, q_e (mg/g) is the amount of dye adsorbed per unit of the adsorbent at equilibrium, V (L) is the volume of dye solution and m (g) is the mass of the adsorbent.

3. Results and discussion

3.1. Characterisation of ZnO nanoparticles

Various diffraction peaks of ZnO nanoparticles at 2θ are 32.1˚, 34.8˚, 36.6˚, 47.9˚, 56.9˚, 63.1˚, 66.7˚, 68.2˚, 69.4˚ resemble the diffraction plane (100), (002), (101), (102), (110), (103), (200), (112), (201) respectively (Fig. 2). A comparison of recorded diffraction peaks of ZnO nanoparticles with standard ZnO proved that synthesized particles are of ZnO [8].

FTIR specta of ZnO nanoparticles is given in Fig. 3(a). The absorption band at region 3400-3700 cm^{-1} may be due to O-H stretching of water molecule. The symmetric and asymmetric stretching vibration peak of C-H bond was observed at 2918 and 2846 cm^{-1}. The sharp bending vibration peak at 1627 and 1653 cm^{-1} was attributed to O-H stretching vibration of water. These vibrations represent the bound water on ZnO nanoparticles. The sharp peak at 1458 cm^{-1} corresponded to O-H stretching vibration [11]. The several weak absorption peaks at range 1550-1380 cm^{-1} could be attributed to the nitrogen and carbon-containing functional groups of precursor (such as C-N, C-H and N-H) and reaction by-products bound on the surface of ZnO. The absorption peaks at 914, 642 and 443 cm^{-1} revealed the presence of Zn-O-H and Zn-O stretching vibration [12].

Fig. 3(b) illustrates the nitrogen adsorption–desorption isotherms and BJH pore size distribution plot of the ZnO nanoparticles. It also exhibits high adsorption at relative pressure (P/P0) greater than 0.8. According to Brunauer-Deming-Deming-Teller (BDDT) classification, the obtained curve related to type VI isotherm, which indicates the mesoporous structure. The BET

surface area of ZnO nanoparticles was found to be 5.6 m^2/g. The pore size distribution curve was determined using BJH methods. The BJH average pore size, total pore volume and pore surface area of ZnO nanoparticles was 28.12 nm, 0.039 cm^3/g and 11.25 m^2/g, respectively. ZnO nanoparticles surface profile was captured at different magnification (10kX and 20kX) using Scanning electron microscope (Figure 4a-b).This captured SEM images showed the prepared ZnO nanoparticles are flower shaped crystal structure. Zn and O energy peaks was observed in EDX spectra of ZnO nanoparticles and its weight (%) and atomic (%) of elements are shown in Figure 4c. The hydrodynamic size distribution of ZnO nanoparticles was analysed by DLS spectra. The size distribution of ZnO nanoparticles was found in the range of 500 to 800nm (Figure 4d). The pH_{pzc} value of synthesized ZnO nanoparticles was obtained from plot between ΔpH and pH_i. In Fig. 5a, pH_{pzc} of ZnO nanoparticle was 6.9 observed at 27˚C. The surface of ZnO carried positive charge at $pH < pH_{pzc}$ and negative charge at $pH > pH_{pzc}$.

3.2. Batch adsorption studies

3.2.1. Effect of pH

Effect of pH on CR and BG dyes removal was studied in the pH range 4-10. All other experimental conditions viz., adsorbent dose 0.04g, CR and BG conc. 50mg/L, temp. 27±1˚C and contact time 2h were constant. In batch mode, CR (anionic) dye removal decreased from 97% to 57% with increase in pH from 4 to10. While BG (cationic) dye removal increased from 53% to 80% with increase in pH. Both cationic and anionic dyes are showed different removal behaviour with pH (Fig. 5b). At lower pH, ZnO nanoparticles carry a positive surface charge due to the protonation (H^+). CR dye molecules contain a negative charge because of an anionic sulfonate group. The pH_{pzc} of synthesized ZnO was 6.9. Hence, at lower pH 4 (below pH_{pzc}), more electrostatic attractions between negatively charged dye molecules and positively charged surface of the ZnO nanoparticles enhance the dye removal. With the increase in pH above 4, CR dye removal was decreased continuously. It may be due to the increase in electrostatic repulsion between negatively charged dye molecule and negatively charged (hydroxyl ions) surface of the ZnO nanoparticles. Similar behaviour of CR removal has been observed by other authors [13, 14]. While in case of BG dye, molecules are positively charged. At low pH, the electrostatic repulsion between BG dye molecules and the positively charged surface of the ZnO nanoparticles is higher that leads to lesser dye removal [1]. With the increase in pH up to 7.0, dye removal increased continuously. There

was no significant increment in dye removal after pH 7.0. The maximum adsorption efficiency of BG dye was achieved at pH 7.0. Therefore, in Fig. 5b the results showed that the electrostatic mechanism was not only the mechanism involved in BG dye adsorption but some other mechanism was also worked. All other dye removal experiments, for both dyes, were performed at pH 6.5±0.5.

3.2.2. Effect of initial dye concentration

The effect of initial dye concentration on the removal of CR and BG dyes was studied with the change in the dye concentration range 10 to 100mg/L. Other experimental conditions such as pH 6.5±0.5, adsorbent dose 0.04g, temp. 27±1˚C and contact time 2h were kept constant. For CR dye, removal was decreased from 98.7% to 54% with the increase in dye concentration. For BG dye, removal decreased from 80% to 73% with an increase in dye concentration (Fig. 5c). Other researchers have also reported similar behaviour with dye concentration [5]. At lower dye concentration (10mg/L), the adsorption efficiency of ZnO nanoparticles was 98.7% and 80% for CR dye and BG dye, respectively (Fig. 5c). This pattern of dye removal may be due to the fact that at lower initial dye concentration, a large number of active sites are available on a surface of ZnO nanoparticles for dye adsorption. However, with the increase in dye concentration, the numbers of surface-active binding sites decreased due to saturation of binding sites by the dye molecules [2].

3.2.3. Effect of Adsorbent dose

The effect of adsorbent dose on dye removal was studied in 50mL dye solution having 50 mg/L dye concentration at 27±1˚C temperature for 150 min. For CR dye, adsorption efficiency continuously increased from 62 to 90% with the increase in adsorbent dose from 0.02 to 0.10g (Fig. 6a).The maximum adsorption efficiency was achieved with 0.10g adsorbent dose. While for BG dye, the adsorption efficiency increased from 65 to 79% with the increase in adsorbent dose from 0.02g to 0.08g and then adsorption equilibrium attained at 0.08g adsorbent dose. The maximum adsorption efficiency (80%) for BG dye observed at 0.08g and 0.10g adsorbent dose. This phenomenon may be due to the fact that the number of available surface active sites increased with increase in adsorbent dose and attain equilibrium to some extent due to agglomeration of the surface active site with the increase in adsorbent dose [5]

3.2.4. Effect of contact time

Effect of contact time on dye removal by ZnO nanoparticles was studied to explore the equilibrium time for dye removal. Adsorption efficiency experiments were carried out with different contact times ranging from 15 to 150 minutes. Almost, similar behaviour was observed for both dyes during experiment. The dye removal increased from 53.4 to 78.6% and 49 to 80% with increase in contact time from 15 to 150 min. for CR dye and BG dye, respectively (Fig. 6b). Initially, fast increase in dye adsorption may be due to availability of large number of free surface active sites on ZnO nanoparticles for dye adsorption. After some instant of time, the adsorption of dye was slow down and finally attained equilibrium.. It may be due to the saturation of adsorbent surface and repulsive force build between dye molecules on adsorbent surface [15, 16].

3.2.5. Effect of temperature

The effect of temperature was studied in the temperature range 10 to 70˚C using a dye solution having 50mg/L dye concentration for 150 min. Cationic and anionic dyes showed opposite adsorption behaviour with temperature (Fig. 6c). In CR dye, the dye removal percentage decreased from 73 to 50% with rise in temperature from 10 to 70˚C due to increase in solubility of anionic dye. This shows the adsorption process is exothermic in nature. It may be attributed to desorption of dye molecules by the internal heat energy of adsorbent at higher temperature [17]. While for BG dye, the removal percentage increased from 51 to 95% with the increase in temperature. This may be due to the increase in mobility and dispersion of dye molecules in solution with temperature which may have enhanced the degree of interaction between dye molecules and surface active sites of ZnO nanoparticles [14].

3.3. Thermodynamic study

Thermodynamic parameters for CR and BG dye adsorption on ZnO nanoparticles are explained using temperature experiments (10˚- 70˚C). Gibb's free energy (ΔG^{o}), entropy (ΔS^{o}) and enthalpy (ΔH^{o}) were calculation by following equations [18]

$$\Delta G^{0} = -RTlnK_{d} \quad (3)$$

$$K_{d} = \frac{C_{a}}{C_{e}} \quad (4)$$

$$lnK_{d} = \frac{\Delta H^{0}}{RT} - \frac{\Delta S^{0}}{R} \quad (5)$$

Where R (8.314 J $mol^{-1}K^{-1}$) is gas constant, K_d is the equilibrium constant, T (K) is the temperature and C_a (mg/L) is the amount of CR and BG dye onto the surface of ZnO nanoparticles at equilibrium.

The slope and intercept values of linear plots between lnK_d versus 1/T used to calculate ΔH° and ΔS°. The negative value of ΔH° (–15.57 kJ mol^{-1}) for CR dye and positive value of ΔH° (41.63 kJ mol^{-1}) for BG dye indicates that the adsorption process is exothermic and endothermic in nature, respectively (Table 2). The results verify that BG dye adsorbed by physical processes [15]. The negative value of ΔS° (– 46.04 J $mol^{-1}K^{-1}$) indicates the decrease in the degree of randomness at the solid-solution interface during CR dye adsorption. The positive value of ΔS° (148.2 J $mol^{-1}K^{-1}$) confirms that the increase in the degree of randomness at the solid-solution interface during BG dye adsorption [19]. Negative values of ΔG° for both the dyes suggest the spontaneity and feasibility of adsorption experiments (Table 2). These thermodynamic parameters value confirm physical-adsorption of dye molecules.

3.4. Kinetic study

The rate mechanism of dye removal process was determined using Pseudo-first order [20], pseudo-second order [21] and intraparticle diffusion [22] Kinetic models. These models are expressed as linear form by following equation.

$$\log(q_e - q_t) = log q_e - \left(\frac{k_1}{2.303}\right) t \quad (6)$$

$$t/q_t = 1/k_2\, q_e^2 + \; t/q_e \quad (7)$$

$$q_t = k_{id}\, t^{1/2} + C \quad (8)$$

Where q_e and q_t (mg/g) are the adsorption capacity at equilibrium times and at time t, respectively, k_1 (min^{-1}) is the kinetic rate constant, k_2 (min^{-1}) is the pseudo-second order rate constant, k_{id} (mg $g^{-1}min^{-1/2}$) is the intra-particle diffusion rate constant and C is the thickness of boundary layer effect. All kinetic parameters values are summarized in Table 3.

In pseudo-first order, the values of k_1, and q_e was determined from plot log (q_e – q_t) versus t. The q_e (cal) value obtained from plot is lower than q_e (exp) value and low linear regression coefficient of CR dye (R^2 = 0.891) and BG dye (R^2 = 0.909) indicates the non-applicability of pseudo-first order for adsorption experiments. Pseudo-second order

regression coefficient (R^2 = 0.985) of both dyes are greater than pseudo-first order. The q_e (cal) value obtained from a plot between t/q_t versus t is closer to q_e (exp) value. Therefore, pseudo-second order equation is better fitted to the data.

In intraparticle diffusion model, k_{id}, C and R^2 values were determined from the plot between q_t versus $t^{1/2}$ (Table 3). If plots don't pass through the origin (C≠0) and not in straight line specify intraparticle diffusion is not only the rate determining step [13]. The obtained value of R^2 and C for both dyes indicates the adsorption process may be controlled by film diffusion and some other mechanism rather than intraparticle diffusion. Hence, intraparticle diffusion model is not applicable to the adsorbing of studied dyes onto ZnO nanoparticles data.

Adsorption isotherms

Adsorption capacity of CR and BG dye on to ZnO was determined at dye concentration range 10 - 100mg/L shown in Fig. 7ab. Adsorption behaviour between dye molecules and adsorbent is explained by Langmuir, Freundlich, Temkin and Dubinin-Radushkevich adsorption isotherms. The linear form of Langmuir isotherms [23] is:

$$\frac{C_e}{q_e} = \frac{1}{q_{max}b} + \frac{C_e}{q_{max}} \tag{9}$$

Where q_{max} (mg/g) is the maximum adsorption capacity, *b* (L/mg) is the Langmuir constant. Adsorption parameters were calculated using linear equation obtained from plots between C_e/q_e versus C_e. Langmuir isotherm parameters and correlation coefficient for CR dye and BG dye are given in Table 4.

Freundlich isotherms models [24] can be represented by below given equation:

$$logq_e = logK_f + \frac{1}{n}\, logC_e \tag{10}$$

Where K_f (mg/g(L/mg)$^{1/n}$) is Freundlich constant and *n* is the heterogeneity factor. The linear plots log q_e versus log C_e to calculate the parameter values. The value of *n* should lie in between 1 to 10 for favourable adsorption process. Freundlich isotherms parameters and correlation coefficients for CR and BG dyes are given in Table 4.

Temkin isotherms model [25] can be represented by following equation

$$q_e = BlnK_T + BlnC_e \tag{11}$$

Where $B = RT/b$, b (J/mol) is the Temkin constant indicates the heat of adsorption, R (8.314 J/molK) is the gas constant, T (K) is absolute temperature and K_T (L/g) is equilibrium binding constant. The values of Temkin parameter were determined by plotting the graph between q_e versus lnC_e. The correlation coefficient and parameter values of CR and BG dyes are given in Table 4.

Dubinin- Radushkevich isotherms [26] model can be represented by below given equation.

$$lnq_e = lnQ_s - K_D\,\varepsilon^2 \quad (12)$$

$$\varepsilon = RT\ln(1 + 1/\mathrm{C_e}) \quad (13)$$

Where Qs (mg/g) is the maximum adsorption capacity, K_D (mol^2/KJ^2) is the activity coefficient indicates the mean adsorption energy, and ε is Polanyi potential which can be calculated from given equation. The values of K_D and Qs were calculated from the slope and intercept obtained from plots between $ln\ q_e$ versus ε. The mean adsorption energy E (KJ/mol) was calculated from the value of K_D by given equation.

$$E = 1/\sqrt{2K_D} \quad (14)$$

The D-R model was applied to the experimental data to explained mean free energy and the characterstics of adsorbents [3]. The D-R model parameters and correlation coefficient of CR and BG dyes are given in Table 4.

The comparison of isotherms models data and parameters indicate that Freundlich model is in good agreement with adsorption experiments data for both the dyes. The correlation coefficient for CR dye (R^2= 0.989) and BG dye (R^2= 0.996) is higher than other studied models. the value of n (n=3.51 for CR and n=1.20 for BG) shows the adsorption process is favourable for both dye. For the experimental data, the multilayer adsorption of both the dyes onto heterogenous active sites of adsorbents can be inferred. The Langmuir maximum adsorption capacity of CR and BG dyes onto ZnO nanoparticles was upto 71.43 mg/g and 238 mg/g respectively. The adsorption capacity of synthesized ZnO nanoparticles for CR and BG dyes are compared to other studied isencapsulated in Tables 5.

3.5. Adsorption mechanism

The study of mechanism of dye adsorption on adsorbent surface is complicated because several factors are involved in the adsorbent-adsorbate interactions. The interaction and binding of dye molecules with adsorbent surface depends upon adsorbent surface

properties, functional groups and molecular structure of dyes. The proposed mechanism may be illustrate by FTIR spectra of ZnO nanoparticles before and after dye adsorption. Before adsorption ZnO nanoparticles IR peak have already been explained in section 3.1. In CR dye adsorbed ZnO nanoparticles (CR-ZnO) a slightly decrease in broad band range at 3300-3600 cm^{-1} revealed the O-H group involved in CR dye adsorption (Fig. 3b). A decrease and shift in peaks at 1600-1700 cm^{-1} was observed after CR dye adsorption. A stretching vibrations at ~1053 cm^{-1} due to the sulfonate group (S=O) was observed after CR dye adsorption. In BG dye adsorbed ZnO nanoparticles FTIR spectra, the increase in band intensity at 3433 cm^{-1} may be due the hydrogen bond interaction between dye molecules and adsorbent surface. After BG dye adsorption some new peaks arise at 1376-1100 cm^{-1} indicate the asymmetrical bending vibration of $–CH_3$ and $–CH_2$ (Fig. 3c). The pH_{pzc} of vaule of ZnO nanoparticles was around 6.9 (Fig. 5a). Above pH 6,9, the surface of ZnO was carried negative charged due to the presence of hyroxyl group. This negative charged surface electrostaticaly interact with cationic species (BG dye) available in solution. The pH below pH_{pzc} 6.9, the surface of ZnO was protonated due to presence of hyrogen ions (H^+). This positive charge favour to electrostatically bind with anionic species (CR dye). These observed results of FTIR, surface charge and pH_{pzc} indicated that the hydrogen bonding and electrostatic intraction was involved in the adsorption of CR and BG dye on the surface of ZnO nanoparticles (34). The possible mechanism of dye adsorption onto ZnO surface was shown in Fig. 8.

3.6. Reusability

The reusability of ZnO nanoparticles was investigated by successive cycles of CR and BG dyes adsorption under different process conditions. For reusability ZnO nanoparticles were separated from the aqueous medium after adsorption experiments. These were washed with ethanol and distilled water several times then dried in hot air oven at 100˚C.This ZnO nanoparticles were again used for adsorption experiments. Three numbers of cycles of adsorbent for both the dyes were run shown inFig. 9. The results showed that CR dye removal (83%) and BG dye removal (90%) was sustained after three cycles of reuse of ZnO nanoparticles.

4. Conclusion

This study shows that the hydrothermally synthesized ZnO nanoparticles are small size, hexagonal crystal structure and flower shape characterized by DLS, XRD, SEM and EDX. These ZnO nanoparticles are efficiently remove both CR and BG dye at pH 6.5±0.5.

Among all studied isotherms models, a Freundlich isotherm is best fitted in experimental data. The maximum adsorption capacity of ZnO nanoparticles for CR and BG dyes was 71.43 mg/g and 238 mg/g, respectively. The rate mechanism of dye adsorption is well described by pseudo-second order model. Thermodynamic study shows that the adsorption of both dyes onto ZnO nanoparticles is spontaneous and physical adsorption. The reusability study explores adsorption capability of ZnO nanoparticles during recycle. The results show that ZnO nanoparticles performance for CR dye (83%) and BG dye (90%) is sustained up to three cycles. Finally, this work concludes that ZnO nanoparticles are eco-friendly and economically efficient adsorbent for both cationic (CR) as well as anionic (CR) dyes. This ZnO nanoparticles can be explores for other dye and dye containing wastewaters treatment.

References

1. V.K. Garg, R. Kumar, R. Gupta, Removal of malachite green dye from aqueous solution by adsorption using agro-industry waste: a case study of Prosopis cineraria, Dyes Pigm. 62 (2004a) 1–10.
2. M.S.U. Rehman, M. Munir, M. Ashfaq, Rashid, N. M.F. Nazar, M. Danish, J.I. Han, Adsorption of Brilliant Green dye from aqueous solution onto red clay, Chem. eng. Sci. 228 (2013) 54–62.
3. M. Ghaedi, A. Ansari, F. Bahari, A.M. Ghaedi, A. Vafaei, A hybrid artificial neural network and particle swarm optimization for prediction of removal of hazardous dye brilliant green from aqueous solution using zinc sulfide nanoparticle loaded on activated carbon. Spectrochim. Acta Mol. Biomol. Spectrosc.137 (2015) 1004–1015.
4. K. Ahmadi, M. Ghaedi, A. Ansari, Comparison of nickel doped Zinc Sulfide and/or palladium nanoparticle loaded on activated carbon as efficient adsorbents for kinetic and equilibrium study of removal of Congo red dye, Spectrochim. Acta Mol. Biomol. Spectrosc.136 (2015) 1441–1449.
5. V.K. Garg, M. Amita, R. Kumar, R. Gupta, Basic dye (methylene blue) removal from simulated wastewater by adsorption using Indian Rosewood sawdust: a timber industry waste, Dyes Pigm. 63 (2004b) 243-250.
6. N.M. Mahmoodi, Zinc ferrite nanoparticle as a magnetic catalyst: synthesis and dye degradation, Mater. Res. Bull. 48 (2013) 4255–4260.
7. K.Y. Kumar, H.B. Muralidhara, Y.A. Nayak, J. Balasubramanyam, H. Hanumanthappa, Low-cost synthesis of metal oxide nanoparticles and their application in adsorption of commercial dye and heavy metal ion in aqueous solution, Powder Technol. 246 (2013) 125–136.
8. X. Wang, W. Cai, S. Liu, G. Wang, Z. Wu, H. Zhao, ZnO hollow microspheres with exposed porous nanosheets surface: Structurally enhanced adsorption towards heavy metal ions, Colloids Surf. A Physicochem Eng Asp. 422 (2013) 199– 205.
9. Y. Kikuchi, Q.R. Qian, M. Machida, H. Tatsumoto, Effect of ZnO loading to activated carbon on Pb(II) adsorption from aqueous solution, Carbon 44 (2006) 195–202.
10. N. Kataria, V.K. Garg, M. Jain, K. Kadirvelu, Preparation, characterization and potential use of flower shaped Zinc oxide nanoparticles (ZON) for the adsorption of Victoria Blue B dye from aqueous solution, Adv. Powder Technol. 27 (2016) 1180–1188.

11. S.M. Mousavi, A.R. Mahjoub, R. Abazari, Green synthesis of ZnO hollow sphere nanostructures by facile route at room temperature with efficient photocatalytic dye degradation, RSC Adv. 5 (2015) 107378-107388
12. S.K. Kansal, R. Lamba, S.K. Mehta, A. Umar, Photocatalytic degradation of Alizarin Red S using simply synthesized ZnO nanoparticles, Mater. Lett. 106 (2013) 385–389.
13. S. Dawood, T.K. Sen, Removal of anionic dye Congo red from aqueous solution by raw pine and acid-treated pine cone powder as adsorbent: Equilibrium, thermodynamic, kinetics, mechanism and process design, Water Res. 46 (2012) 1933-1946.
14. M.A.M. Salleh, D.K. Mahmoud, W.A. Karim, A. Idris, Cationic and anionic dye adsorption by agricultural solid wastes: a comprehensive review, Desalination 280 (2011) 1-13.
15. B.K. Nandi, B.K. Goswami, M.K. Purkait, Adsorption characteristics of brilliant green dye on kaolin, J Hazard. Mater. 161(2009) 387–395.
16. V.S. Mane, P.V.V. Babu, Studies on the adsorption of Brilliant Green dye from aqueous solution onto low-cost NaOH treated saw dust, Desalination 273 (2011) 321–329.
17. J. Saini, V.K. Garg, R.K. Gupta, N. Kataria, Removal of Orange G and Rhodamine B dyes from aqueous system using hydrothermally synthesized zinc oxide loaded activated carbon (ZnO-AC), Journal of Environmental Chemical Engineering 5 (2017) 884–892.
18. J.M. Smith, H.C.V. Ness, Introduction to Chemical Engineering Thermodynamics. McGraw-Hill New York, USA. (1987)
19. W. Zou, K. Li, H. Bai, X. Shi, R. Han, Enhanced Cationic Dyes Removal from Aqueous Solution by Oxalic Acid Modified Rice Husk, J. Chem. Eng. Data 56 (2011) 1882–1891.
20. S. Lagergren, Kung. Sven. Veten. Hand. 24 (1898) 241–39.
21. Y.S. Ho, J.C.Y. Ng, G. Mckay, Kinetics of pollutants sorption by biosorbents: review, Sep. Purif. Method 29 (2000) 189–232.
22. W.J. Weber, J.C. Morris, Kinetics of adsorption on carbon from solution, J. Sanitary Eng. Div. Am. Soc. Civ. Eng. 89 (1963) 31–60.
23. I. Langmuir, The constitution and fundamental properties of solids and liquid, J. Am. Chem. Soc 38 (1916) 2221–2295.
24. H.M.F. Freundlich, over the adsorption in solution, J. Phys. Chem 57, (1906) 385–471.
25. M.J. Temkin, V. Pyzhev, Recent modification to Langmuir isotherms, Acta Physiochim USSR 12 (1940) 217–222.
26. M.M. Dubinin, L.V. Radushkevich, Equation of the characteristic curve of activated charcoal, Chem. Zentr. 1 (1947) 875–890.

27. T. Calvete, E.C. Lima, N.F. Cardoso, S.L.P. Dias, E.S. Ribeiro, Removal of Brilliant Green Dye from Aqueous Solutions Using Home Made Activated Carbons, CLEAN – Soil, Air, Water 38 (2010) 521–532.
28. M. Jamshidi, M. Ghaedi, K. Dashtian, A.M. Ghaedi, S. Hajati, A. Goudarzi, E. Alipanahpour, Highly efficient simultaneous ultrasonic assisted adsorption of brilliant green and eosin B onto ZnS nanoparticles loaded activated carbon: Artificial neural network modeling and central composite design optimization, Spectrochim. Acta Mol. Biomol. Spectrosc. 153 (2016) 257–267.
29. J. Zolgharnein, M. Bagtash, T. Shariatmanesh, Simultaneous removal of binary mixture of Brilliant Green and Crystal Violet using derivative spectrophotometric determination, multivariate optimization and adsorption characterization of dyes on surfactant modified nano-c-alumina, Spectrochim. Acta Mol. Biomol. Spectrosc. 137 (2015) 1016–1028.
30. F.A. Pavan, S.L.P. Dias, E.C. Lima, E.V. Benvenutti, Removal of Congo red from aqueous solution by anilinepropylsilica xerogel, Dyes Pigm. 76 (2008) 64–69.
31. M. Ghaedi, M.N. Biyareh, S.N. Kokhdan, S. Shamsaldini, R. Sahraei, A. Daneshfar, S. Shahriyar, Comparison of the efficiency of palladium and silver nanoparticles loaded on activated carbon and zinc oxide nanorods loaded on activated carbon as new adsorbents for removal of Congo red from aqueous solution: Kinetic and isotherm study, Mater. Sci. Eng. C. 32 (2012) 725–734
32. L. Wang, L. Li, Y. Wang, L. Zhao, Q. Jiang, Adsorption capability for Congo red on nanocrystalline MFe_2O_4 (M = Mn, Fe Co, Ni) spinel ferrites, Chem. Eng. J. 181 (2012) 72–79.
33. R. Rahimi, H. Kerdari, M. Rabbani, M. Shafiee, Synthesis, characterization and adsorbing properties of hollow $ZnFe_2O_4$ nanospheres on removal of Congo red from aqueous solution, Desalination 280 (2011) 412–418.
34. S. Dhanavel, E.A.K. Nivethaa, K. Dhanapal, V.K. Gupta, V. Narayanan, A. Stephen, α-MoO 3/polyaniline composite for effective scavenging of Rhodamine B, Congo red and textile dye effluent, RSC Adv. 34 (2016) 28871-28886.

Caption of figures:

Figure 1 Scheme of ZnO nanoparticles synthsis.

Figure 2 XRD patterns of synthesized ZnO nanoparticles.

Figure 3(a) FTIR spectra of synthesized ZnO nanoparticles a) Before adsorption ZnO nanoparticles b) After adsorption CR-ZnO c) After adsorption BG-ZnO. 3(b) Nitrogen adsorption (black filled squares)–desorption (red filled sphere) isotherms of ZnO nanoparticles and inset BJH pore size distribution plot of ZnO nanoparticles Figure 4 (a,b) SEM image at different magnification (c) EDX spectrum and (d) DLS pattern of synthesized ZnO nanoparticles.

Figure 5 (a) Point zero charge (pH_{pzc}) plots ΔpH vs pHi, ZnO, (b) Effect of pH on adsorption of CR and BG dye on ZnO and (c) Effect of dye concentration on adsorption of CR and BG dye on ZnO nanoparticles.

Figure 6 (a) Effect of adsorbent dose on removal of CR and BG dye by synthesized ZnO nanoparticles. (b) Effect of contact time on adsorption CR and BG dye on ZnO nanoparticles and (c) Effect of temperature on adsorption process CR and BG dye.

Figure 7 Adsorption isotherms for CR and BG dye onto ZnO nanoparticles. (pH – 6.5±0.5, dye conc. 10- 100 mg/L, temp.- 27±1˚C, adsorbent dose- 0.04g and time-120min.)

Figure 8 Possible adsorption mechanism of CR and BG dye onto ZnO.

Figure 9 Reusability of ZnO nanoparticles for CR and BG dyes (dye conc.-30 mg/L, pH-natural, temp- 27±˚C, dose- 0.05g and time- 150 min.)

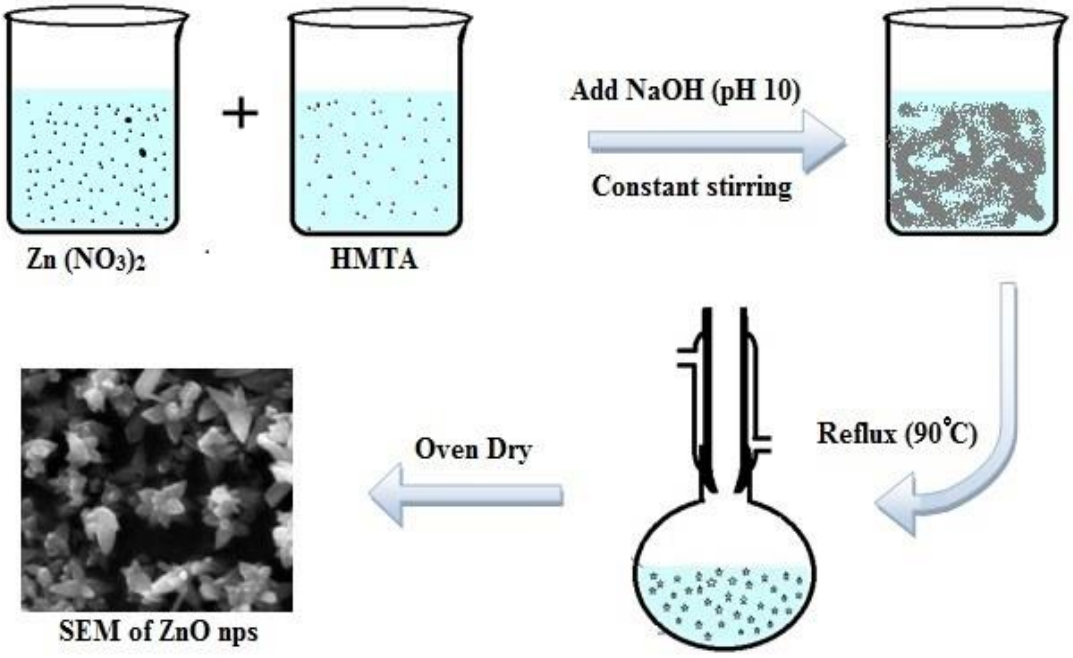

Figure 1 Scheme of ZnO nanoparticles synthsis

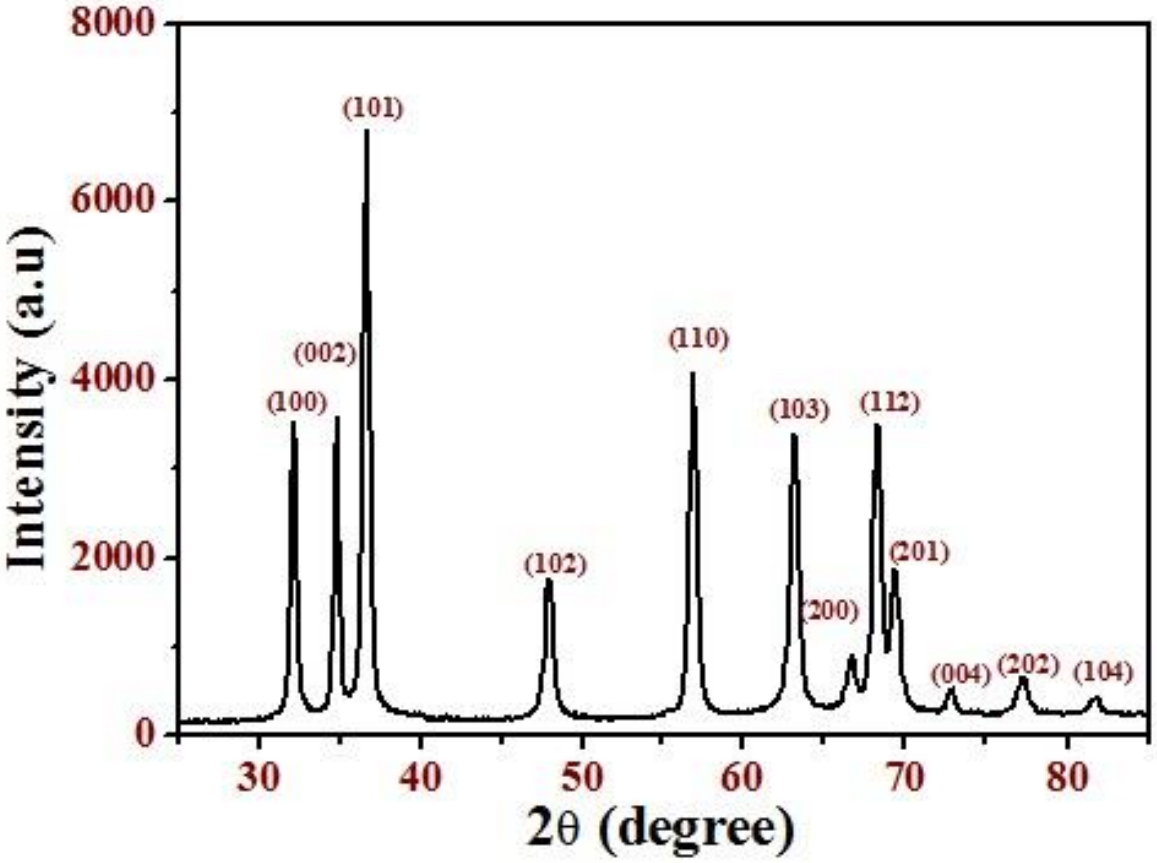

Figure 2 XRD patterns of synthesized ZnO nanoparticles.

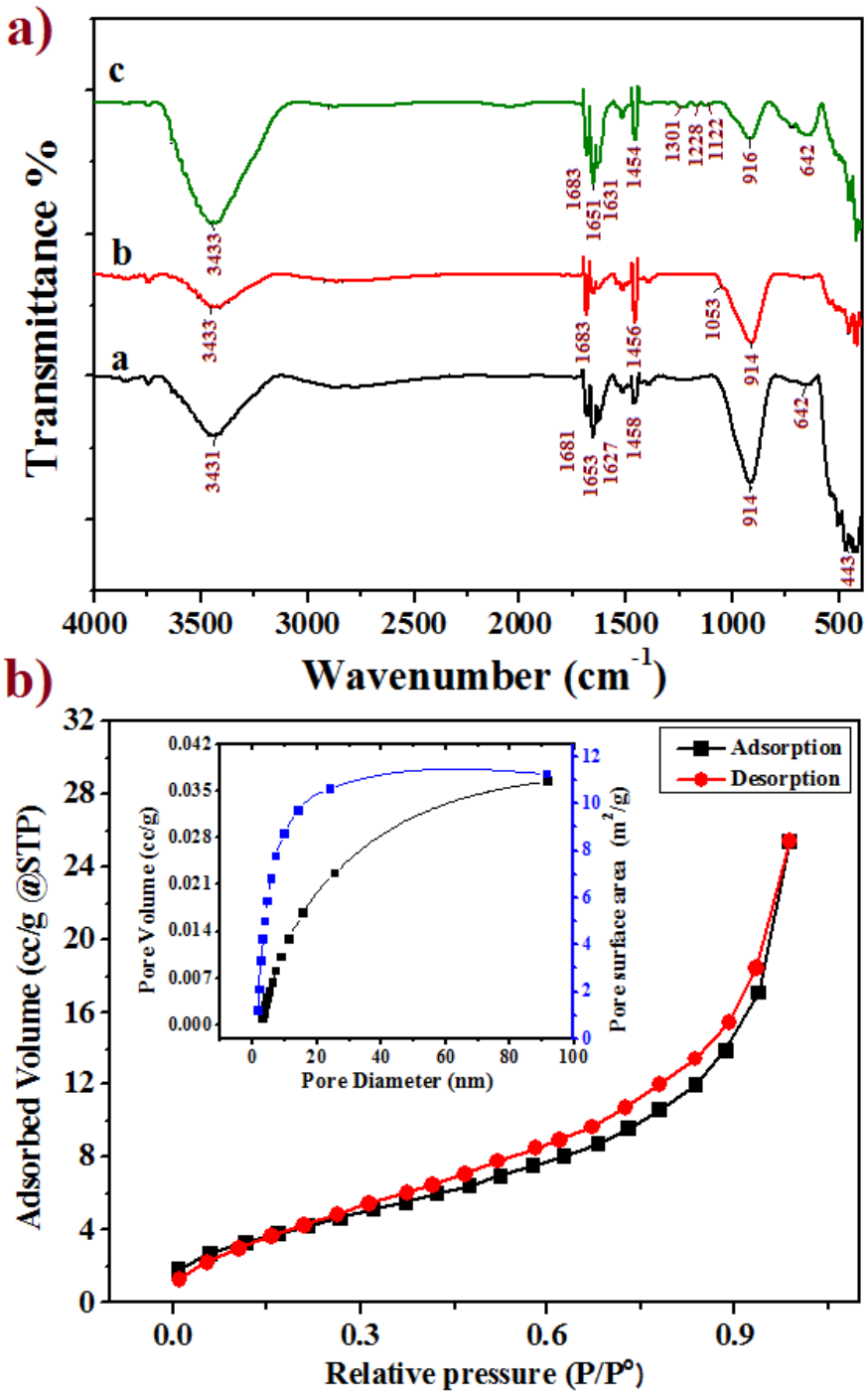

Figure 3(a) FTIR spectra of synthesized ZnO nanoparticles a) before adsorption ZnO nanoparticles b) after adsorption CR-ZnO c) after adsorption BG-ZnO. 3(b) Nitrogen adsorption (black filled squares)–desorption (red filled sphere) isotherms of ZnO nanoparticles and inset BJH pore size distribution plot of ZnO nanoparticles

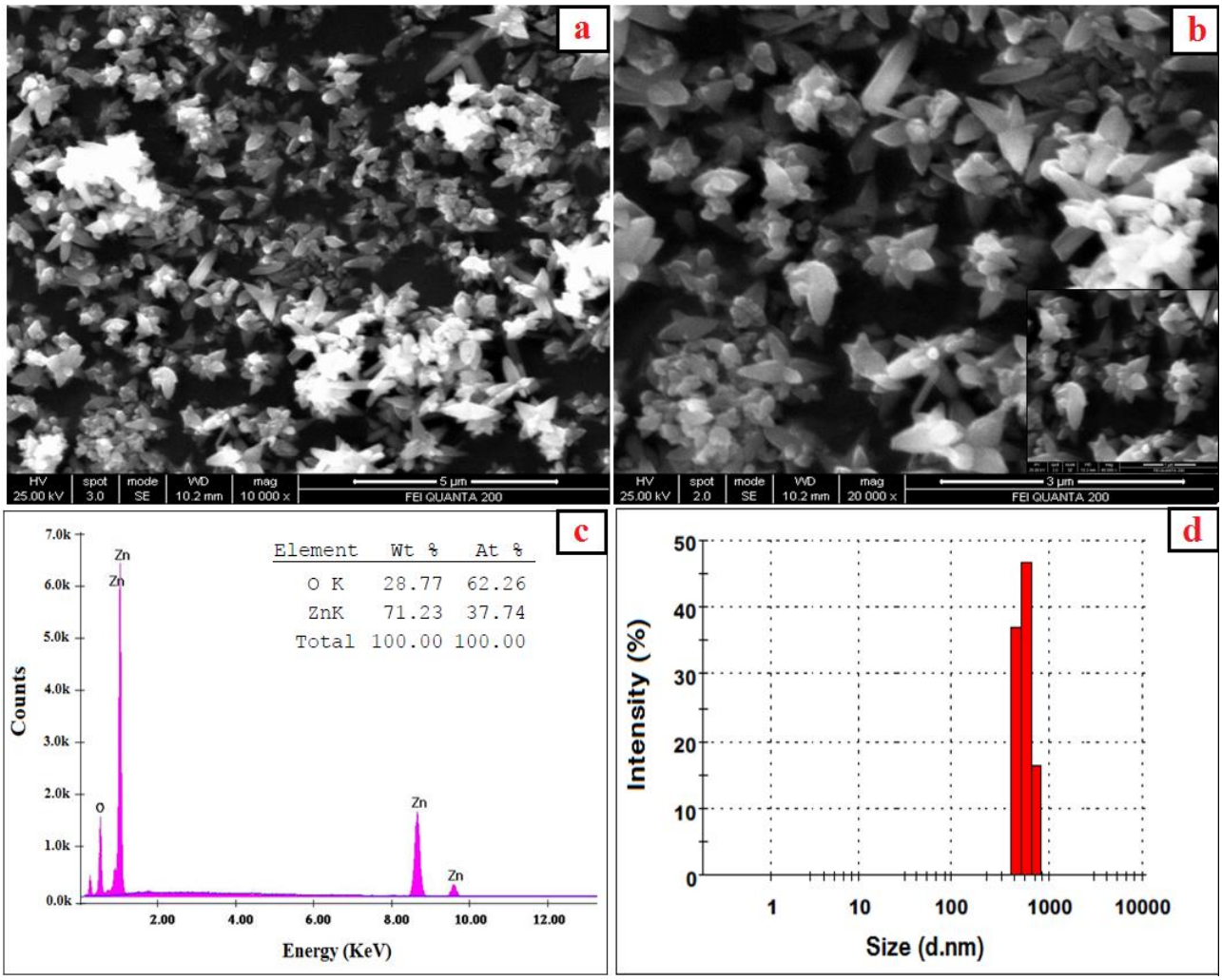

Figure 4 (a,b) SEM image at different magnification (c) EDX spectrum and (d) DLS pattern of synthesized ZnO nanoparticles.

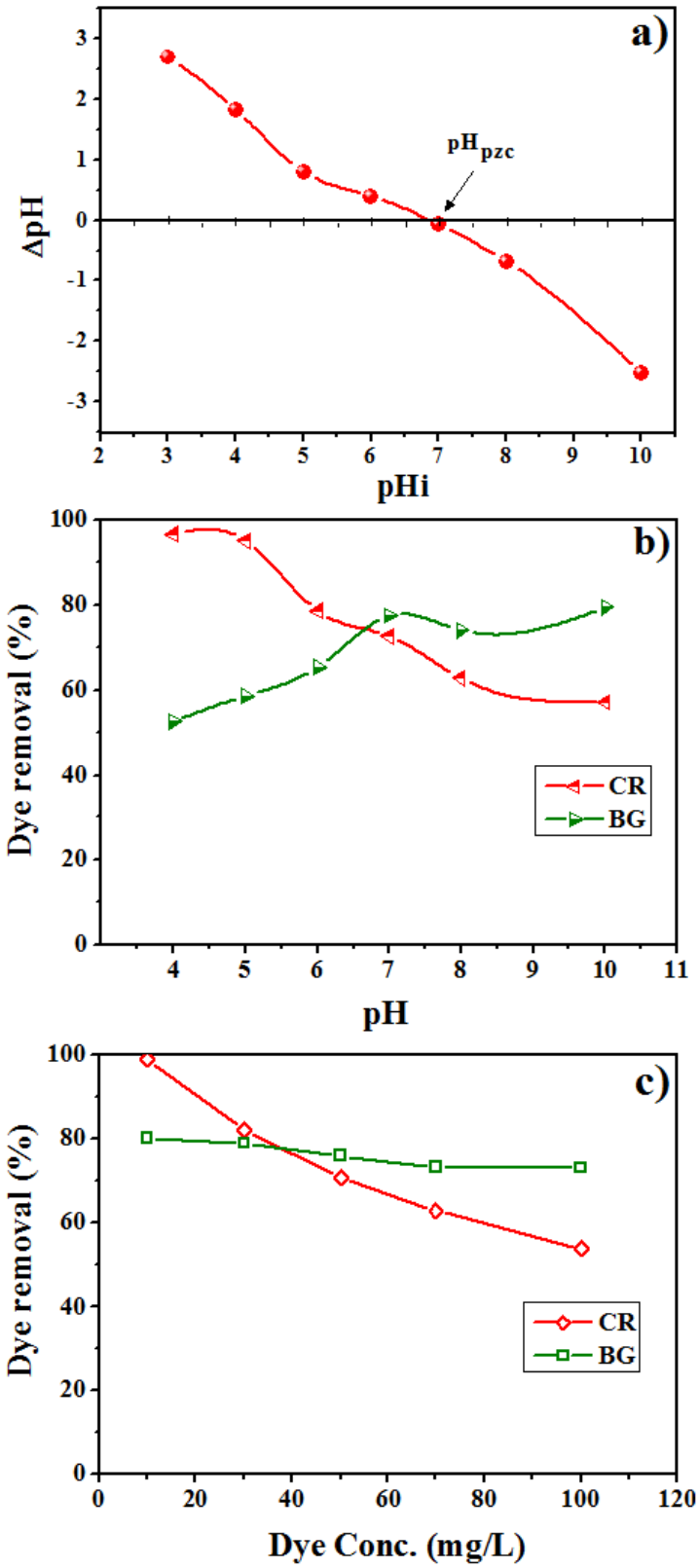

Figure 5 (a) (a) Point zero charge (pH_{pzc}) plots ΔpH vs pHi, ZnO, (b) Effect of pH on adsorption of CR and BG dye on ZnO nanoparticles and (c) Effect of dye concentration on adsorption of CR and BG dye on ZnO nanoparticles.

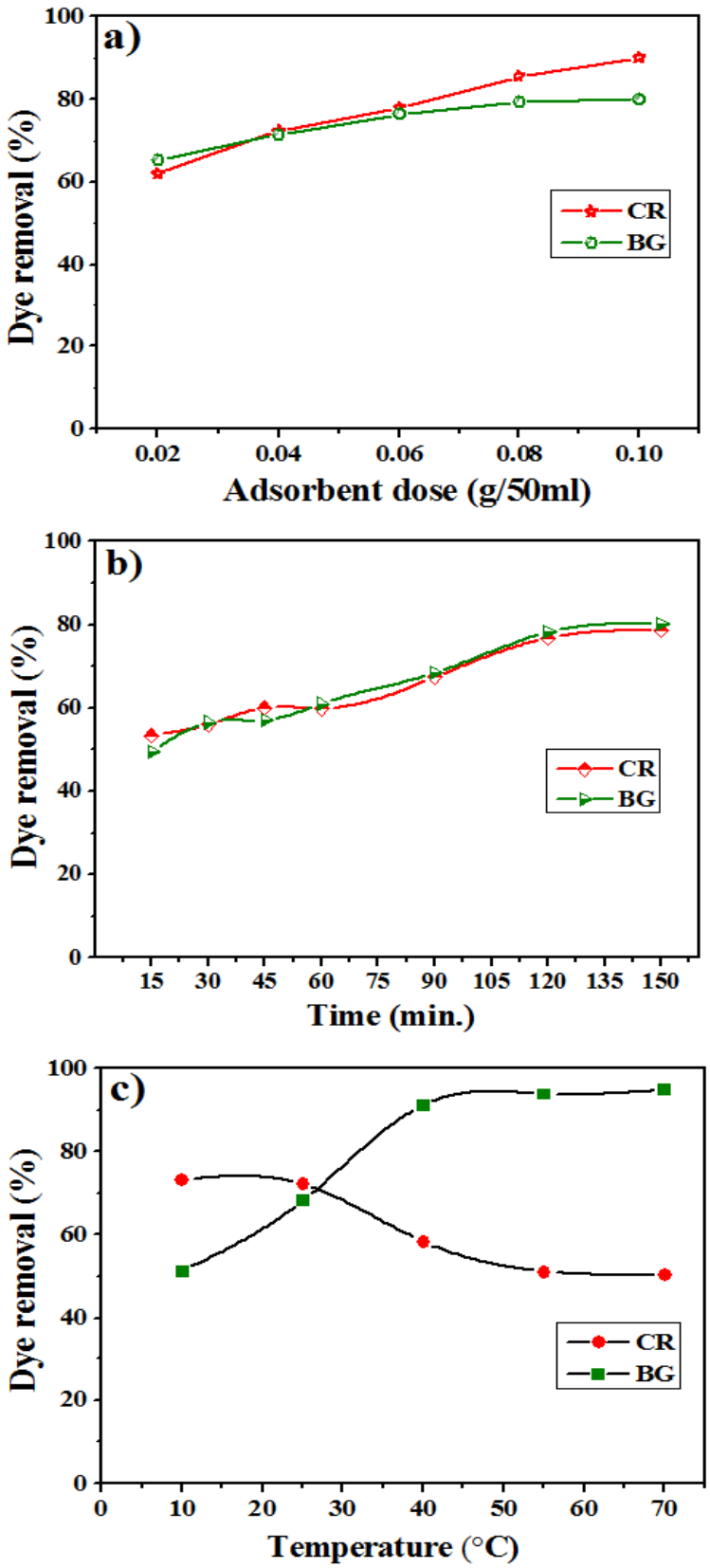

Figure 6 (a) Effect of adsorbent dose on removal of CR and BG dye by synthesized ZnO nanoparticles. (b) Effect of contact time on adsorption CR and BG dye and (c) Effect of temperature on adsorption process CR and BG dye on ZnO nanoparticles.

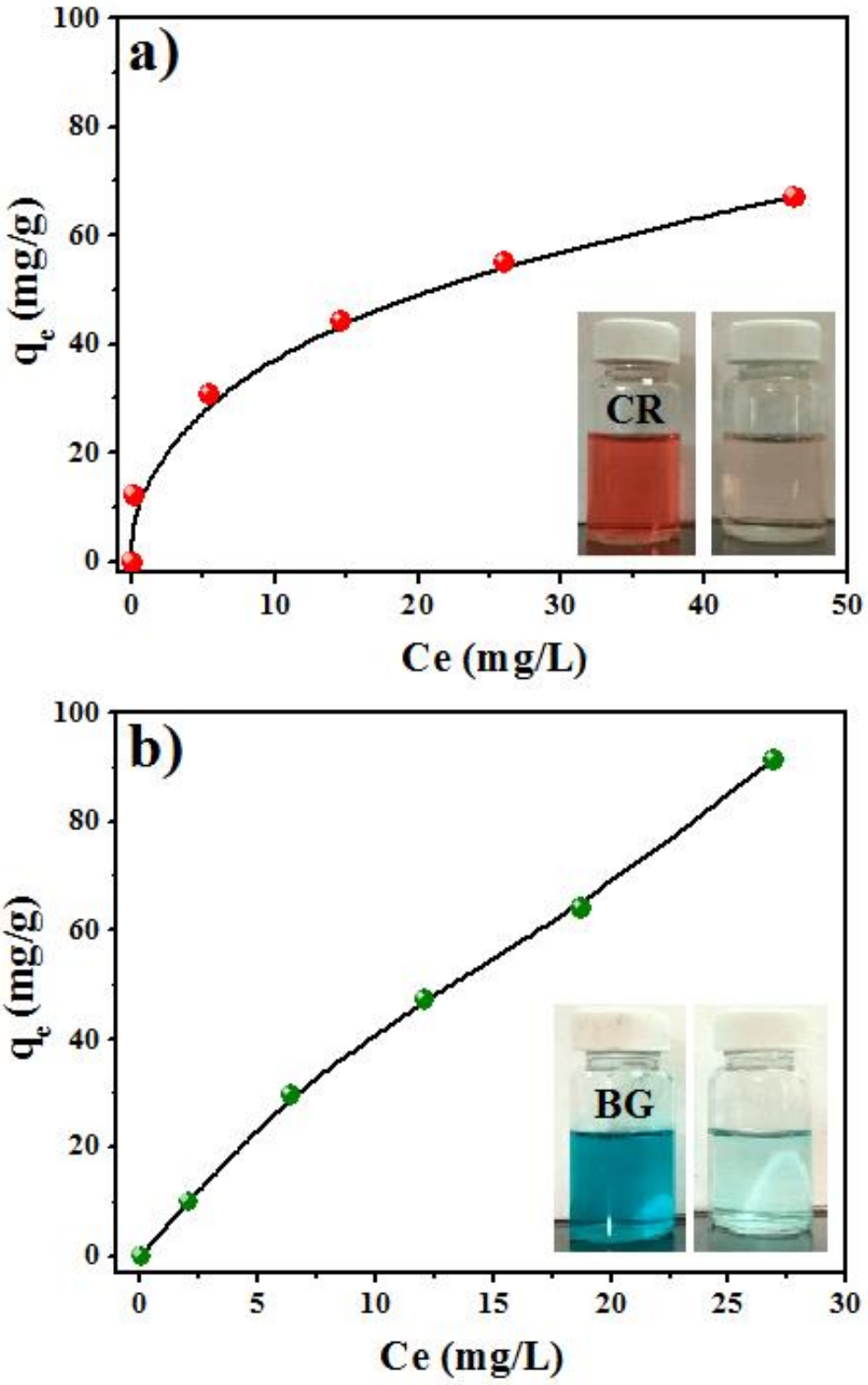

Figure 7 Adsorption isotherms for (a) CR (red line) and (b) BG (green line) dye onto ZnO nanoparticles. (pH – 6.5±0.5, dye conc. 10- 100 mg/L, temp.- 27±1˚C, adsorbent dose- 0.04g and time-120min.)

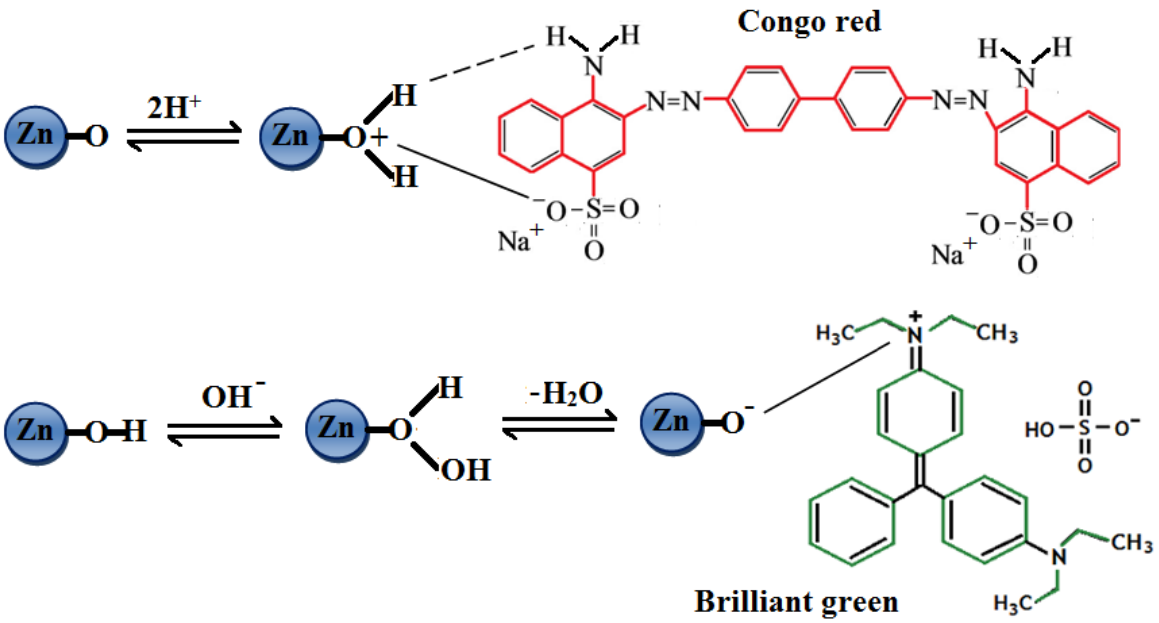

Figure 8 Possible adsorption mechanism of CR and BG dye onto ZnO nanoparticles

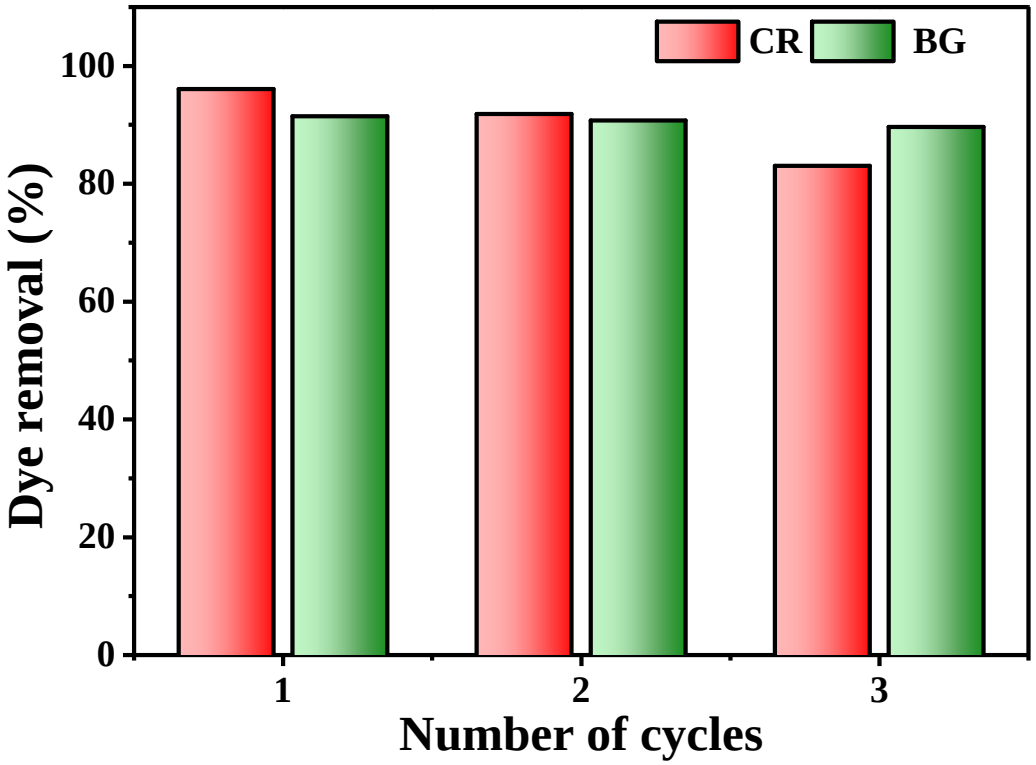

Figure 7 Reusability of ZnO nanoparticles for CR and BG dyes removal (dye conc.-30 mg/L, pH- natural, temp- 27±˚C, dose- 0.05g and time- 150 min.)

Table 1 Properties and structure of Congo red (CR) and Brilliant green (BG) dyes.

Dyes	**Congo red (CR)**	**Brilliant green (BG)**
Molecular formula and structure	$C_{32}H_{22}N_6Na_2O_6S_2$ 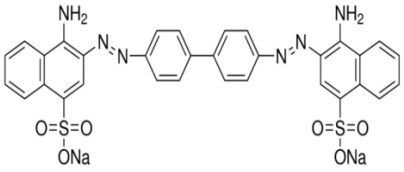	$C_{27}H_{34}N_2O_4S$ 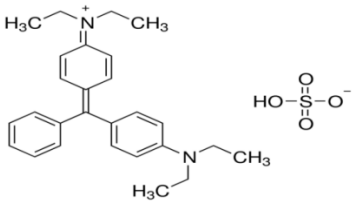
Molecular weight (g/mole)	696.66	482.63
Classification	Azo dye (N=N)	Basic dye
C.I. No	22120	42040
C.I. Name	Direct red 28	Basic green 1
Melting point (˚C)	>360	210
λ_{max} (nm)	497	625

Table 2
Thermodynamic parameter description for CR and BG dye adsorption over ZnO nanoparticles.

Temp. (K)	**Congo Red (CR) dye**			**Brilliant Green (BG) dye**		
	ΔG^o ($kJmol^{-1}$)	**ΔS^o ($Jmol^{-1}K^{-1}$)**	**ΔH^o ($kJmol^{-1}$)**	**ΔG^o ($kJmol^{-1}$)**	**ΔS^o ($Jmol^{-1}K^{-1}$)**	**ΔH^o ($kJmol^{-1}$)**
283	-2.364	- 46.041	-15.568	-0.132	148.222	41.632
298	-2.365			-1.890		
313	-0.883			-6.085		
328	-0.131			-7.408		
343	-0.046			-8.279		

Table 3 Kinetic models parameters study for CR and BG dye adsorption on ZnO nanoparticles.

Kinetic models	**Parameters**	**Values of parameters**	
		CR	**BG**
Pseudo-first order	k_1 (min^{-1})	0.023	0.024
	q_e (cal)	31.12	36.54
	R^2	0.891	0.909
Pseudo-second order	k_2 (g/mg min)	0.0011	0.0009
	q_e (cal)	53.48	55.56
	R^2	0.985	0.985
Intraparticle diffusion	k_{id} (mg $g^{-1}min^{-1/2}$)	2.020	2.375
	C	24.06	21.07
	R^2	0.947	0.969
Experimental data	q_e (exp)	49.10	50.10

Table 4 Adsorption isothermal model for CR and BG dye adsorption on ZnO nanoparticles interpreted by correlation coefficients and adsorption parameters.

Isotherms model	**Parameters**	**Parameters values**	
		CR	**BG**
Langmuir	q_{max} (mg/g)	71.43	238.10
	b (L/mg)	0.182	0.021
	R^2	0.964	0.914
Freundlich	n	3.51	1.20
	K_f (mg/g(L/mg)$^{1/n}$)	21.14	5.83
	R^2	0.989	0.996
Temkin	b	289.46	85.21
	K_T (L/mg)	19.76	0.55
	R^2	0.889	0.914
Dubinin- Radushkevich	Q_s (mg/g)	47.64	59.58
	K_D (mol^2/KJ^2)	5 x 10^{-8}	2 x 10^{-6}
	E (KJ/mol)	100	15.81
	R^2	0.816	0.848

Table 5 Comparative study in adsorption capacity of various adsorbents for CR and BG dyes.

Adsorbent	**Dyes removed**	**$q_{max.}$ (mg/g)**	**Reference**
CAC	BG	219	[27]
CPAC	BG	263	
ZnS-NP-AC	BG	250	[28]
Surfactant modified alumina	BG	168	[29]
ZnS-NP-AC	BG	142.9	[3]
Red clay	BG	125	[2]
Anilinepropylsilica xerogel	CR	22.62	[30]
Raw pine cone	CR	32.65	[13]
Acid-treated pine cone	CR	40.19	
Ag-NP-AC	CR	66.67	[31]
Pd-NP-AC	CR	76.92	
ZnO-NP-AC	CR	142.9	
Fe_3O_4	CR	68.5	[32]
$MnFe_2O_4$	CR	92.4	
$ZnFe_2O_4$	CR	16.1	[33]
ZnO nanoparticles	CR	71.43	present study
ZnO nanoparticles	BG	238.1	present study